ISTITUTO DI ANALISI DEI SISTEMI ED INFORMATICA
CONSIGLIO NAZIONALE DELLE RICERCHE

A. Bertuzzi, A. d'Onofrio, A. Fasano, A. Gandolfi

REGRESSION AND REGROWTH OF TUMOUR CORDS FOLLOWING SINGLE-DOSE ANTICANCER TREATMENT

R. 576 Ottobre 2002

Alessandro Bertuzzi – Istituto di Analisi dei Sistemi ed Informatica del CNR, viale Manzoni 30 - 00185 Roma, Italy. Email : bertuzzi@iasi.cnr.it.

Alberto d'Onofrio – European Institute of Oncology, Division of Epidemiology and Biostatistics, Via Ripamonti 435 - 20141 Milano, Italy. Email : alberto.d'onofrio@ieo.it.

Antonio Fasano – Dipartimento di Matematica "U. Dini", Università di Firenze, viale Morgagni 67/A - 50134 Firenze, Italy. Email : fasano@math.unifi.it.

Alberto Gandolfi – Istituto di Analisi dei Sistemi ed Informatica del CNR, viale Manzoni 30 - 00185 Roma, Italy. Email : gandolfi@iasi.cnr.it.

This work was partially supported by CIMAB, Italy.

ISSN: 1128–3378

Collana dei Rapporti
dell'Istituto di Analisi dei Sistemi ed Informatica, CNR

viale Manzoni 30, 00185 ROMA, Italy

tel. ++39-06-77161
fax ++39-06-7716461
email: iasi@iasi.rm.cnr.it
URL: http://www.iasi.rm.cnr.it

Abstract

In this paper, the evolution of a tumour cord after treatment is investigated by extensive numerical simulations on the basis of a mathematical model developed in Bertuzzi *et al.* (submitted). The model is formulated in cylindrical symmetry adopting the continuum approach, and takes into account the influence of oxygen level on the proliferation and death rate of cells, the volume reduction due to disgregation of dead cells, and the cell killing effects of radiation and drugs. Some extensions of the model are proposed to represent more accurately the radioresistance of hypoxic cells and the cytotoxic action of anticancer drugs. The steady state of the cord, and the cord evolution from the steady state after the delivery of a single dose of an anticancer agent, are computed for various combinations of model parameters and for different choices of the functions describing the effects of treatments. The results of the numerical computations show that, in spite of its many simplifications, the model behaviour appears to be reasonable in view of the available experimental observations. The model allows having a better insight into some complex treatment-related events, such as cell reoxygenation and repopulation.

Key words: Cell populations, tumour cord, response to treatment, free boundary problems.

1. Introduction

The microarchitecture of most solid tumours is very complex, with regions of viable cells intermingled with regions of necrosis, in relation to the irregular and poorly effective vascular network that supplies the tumour. In some human and experimental tumours, however, it is possible to observe tumour cells arranged in cylindrical structures around central blood vessels and surrounded by necrosis. These structures are named tumour cords (Tannock, 1968; Hirst and Denekamp, 1979; Hirst *et al.*, 1982; Moore *et al.*, 1984; Moore *et al.*, 1985; Falkvoll, 1990; Hirst *et al.*, 1991). The mean thickness of the cords (*i.e.*, the distance between the vessel wall and the first layer of necrotic cells) has been reported to be $60 - 130\,\mu$m in different tumours, with mean radius of the central vessel of $10 - 40\,\mu$m. Cell proliferation within the tumour cord induces migration of cells towards the periphery: cells are pushed by the growing and dividing cells and eventually move into the necrotic zone. A marked decrease of cell proliferation with increasing distance from the vessel has been evidenced by experiments using tritiated thymidine to label S-phase cells (Tannock, 1968; Hirst and Denekamp, 1979; Moore *et al.*, 1984). Oxygen and/or nutrient deprivation in the cells remote from the central vessel are likely to play a central role in the decrease of proliferation rate within the cord and in the occurrence of necrosis. Cuffs of tumour cells around vessels of the host, surrounded by host tissue, have been also observed as a characteristic form of micrometastases (Folkman, 1995; Holmgren *et al.*, 1995) and in the initial growth of tumours that involves the cooption of host vessels (Holash *et al.*, 1999). The response of tumour cords to a single dose of radiation or drugs was investigated by Tannock and Howes (1973), Moore *et al.* (1980, 1983) and Falkvoll (1990). The general pattern of the response showed a regression of the cord radius followed by a regrowth phase towards the unperturbed value.

A mathematical model that describes the spatial distribution of the proliferating cells (represented as an age-dependent cell population) and of the quiescent cells in a tumour cord, has been recently proposed (Bertuzzi and Gandolfi, 2000; Webb, 2002). The authors studied the stationary state in the case in which the fraction of newborn cells that become quiescent is a given function of the distance from the blood vessel. The possibility that the progression rate through cell cycle be dependent on the distance from vessels has been also investigated by representing the cell cycle as a sequence of maturity compartments (Bertuzzi *et al.*, 2002) or by means of continuous maturity (Dyson *et al.*, in preparation). The growth of an isolated tumour cord within the normal tissue has been analyzed by Bloor and Wilson (1997, 1999) and Bertuzzi *et al.* (2000). All these models use a quite elementary representation of tumour and normal tissues and include the diffusion and consumption of the nutrient. Whereas the former models consider growth without necrosis formation, in the latter model necrosis formation is described. The longitudinal expansion of the cord has been modeled in Bloor and Wilson (1999).

Mathematical models of the response of spherical tumours to anticancer drugs have been recently developed by Jackson and Byrne (2000), Jackson (2002), and Ward and King (2003). A model of a fully developed system of tumour cords under the influence of cell killing agents was proposed in Bertuzzi *et al.* (submitted). The existence of a unique stationary state in the absence of therapy was established, as well as the existence and uniqueness of the solution of the evolutive problem that arises following the treatment. In the present paper some extensions of the model are proposed, with the aim of representing more accurately the radioresistance of hypoxic cells and the cytotoxic action of anticancer drugs, and the behaviour of the model is extensively investigated by numerical computation of the solutions. Particular emphasis is put on the pivotal role of some peculiar features of the model and on how sensitive the solutions are

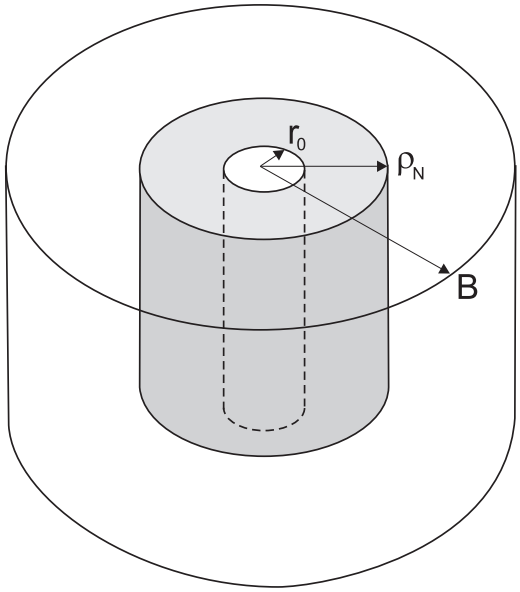

Fig. 1. Schematic geometry of the tumour cord (symbols explained in the text).

to the main parameters characterizing the treatment. Some comparisons with experimental data are included. The model is described in sections 2 and 3 and the numerical results are presented in sections 4 and 5. Appendix A illustrates some details of the computational procedure.

2. Main assumptions

Let us consider an array of tumour cords inside a tumour mass, each cord being separated from others by a region of necrosis. We concentrate on a cord in the core of the system, and we describe the cord as a circular cylinder around a central blood vessel, surrounded by a co-axial cylindrical region of necrosis whose outer boundary is supposed to prevent any exchange of matter with the neighboring cords. This latter assumption is justifiable by symmetry, viewing the cord inside a regular array of parallel identical cords, according to the Krogh model of microcirculation. We denote by r the radial distance from the axis, by r_0 the radius of the central vessel, by $\rho_N(t)$ the cord radius, *i.e.* the interface with the necrotic region, and by $B(t)$ the outer boundary of the necrotic region (see Fig. 1).

We will distinguish three components in the cord and in the necrotic region: viable tumour cells, dead cells and extracellular fluid. We adopt a simplified representation of the cell population by disregarding the cell age or the structure of the cell cycle. Assuming that viable cells, dead cells and extracellular fluid have equal mass densities, we only consider the volume fractions occupied locally by these components under the continuum hypothesis. These fractions are denoted as ν_V, ν_N and, respectively, ν_E (with $\nu_V+\nu_N+\nu_E$ equal to one). In the cord it will be $\nu_V>0$, whereas in the surrounding necrotic zone only dead cells and extracellular fluids will be present and $\nu_V=0$. In this study only the cell killing effects of anticancer treatments are taken into account. We do not consider indeed the cytostatic effects, *i.e.* the induction of reversible blocks in the cell cycle of tumour cells. Moreover, we assume that the treatment does not affect the tumour vasculature, so that the model is restricted to represent rather mild treatments.

The main assumptions of the model are summarized as follows: *(i)* Cylindrical symmetry is assumed, and all the variables describing the cell population state, the cell velocity and the concentrations of chemicals are independent of the axial coordinate. *(ii)* Cell velocity is radially directed. *(iii)* Oxygen is the only species of "nutrient" considered and we do not distinguish the intracellular from the extracellular concentration. We denote by $\sigma(r,t)$ the local oxygen concentration. *(iv)* The rate of cell proliferation, $\chi(\sigma)$, is a nondecreasing function of σ. More precisely, we assume that for σ greater than a given threshold σ_P the cells are fully proliferating and $\chi(\sigma)=\chi_0$. Below σ_P, the progression through cell cycle slows down and/or the fraction of quiescent cells increases, so that $\chi(\sigma)$ is decreasing. Below σ_Q ($\sigma_Q<\sigma_P$) all cells become quiescent and $\chi(\sigma)=0$. If σ increases over σ_Q, all cells resume instantaneously the proliferative status. *(v)* Cells die if σ falls to a threshold value σ_N ($\sigma_N<\sigma_Q$). In addition, random cell death, either spontaneous and induced by treatments, may occur within the cord. *(vi)* The rate of spontaneous cell death, $\mu(\sigma)$, is a non-increasing function of σ, $\mu(\sigma)\in[\mu_{min},\mu_{max}]$. *(vii)* Dead cells are degraded to a fluid waste at a rate μ_N within the cord and at a rate $\tilde{\mu}_N$ in the necrotic region. This waste will be drained away by the flow of extracellular fluid along the axial direction of the cord.

Concerning the above assumptions, we note the following. The consideration of only one species of nutrient is mainly due to simplicity reasons and it was also adopted in other mathematical models of tumour growth (Greenspan, 1972; McElwain and Ponzo, 1977; Adam and Maggelakis, 1990; Byrne and Chaplain 1995, 1996; Cui and Friedman, 2001; Breward *et al.*, 2001, 2002). Neglecting the longitudinal cell motion is a simplification that is justifiable away from the ends of the cord. Moreover the greater importance of radial cell migration in tumour cords has been suggested by Tannock (1968). The different values of the degradation rates μ_N and $\tilde{\mu}_N$ can reflect the different modes of cell death, *i.e.* apoptosis within the cord versus necrosis when σ falls to the death threshold. A slower degradation of necrotic cells with respect to apoptotic cells has been evidenced (Majno and Joris, 1995; Darzynkiewicz *et al.*, 1997).

To represent the cell motion, the dynamics of the mixture of cells and extracellular fluids should be described by writing the momentum balance and including the interactions among the components (Ambrosi and Preziosi, 2002; Lubkin and Jackson, 2002; Breward *et al.*, 2002). To avoid new assumptions necessary to express the stress tensor and to take full advantage of the simplified geometry, we make instead the further simplifying assumptions: *(viii)* The velocity of the cellular component is the same for both living and dead cells. This common velocity is given by the scalar field $u(r,t)$. *(ix)* The volume fraction ν_E of extracellular fluid is constant in space and time. In other words, it is assumed that both viable and dead cells possess a uniform spatial arrangement, which is quickly recovered after any perturbation caused by cell proliferation and liquefaction of dead cells. These assumptions will lead to a purely kinematic approach, as in our previous papers on this subject, and have also been adopted in papers on the growth of avascular (Ward and King, 1997, 1999, 2003) and vascular tumours (Jackson and Byrne, 2000).

3. Model equations

On the basis of the above assumptions, the conservation equations for the volume fractions of viable and dead cells in $r_0 < r < \rho_N(t)$ can be written as follows:

$$\frac{\partial \nu_V}{\partial t} + \mathrm{div}(u\,\nu_V) = \chi(\sigma)\nu_V - [\mu(\sigma) + \mu_R(\sigma,t) + \mu_C(c,\sigma)]\,\nu_V\,, \tag{1}$$

$$\frac{\partial \nu_N}{\partial t} + \mathrm{div}(u\,\nu_N) = [\mu(\sigma) + \mu_R(\sigma,t) + \mu_C(c,\sigma)]\,\nu_V - \mu_N\nu_N\,. \tag{2}$$

In equations (1)-(2), μ_R is the death rate induced by radiation and μ_C is the death rate induced by a drug, $c(r,t)$ being the concentration of the cytotoxic chemical. The dependence of μ_R on t takes into account the schedule of radiation treatment and the delayed effects following the delivery of a single dose, and the dependence on $\sigma(r,t)$ the different radiosensitivity of hypoxic cells. The dependence of μ_C on $\sigma(r,t)$ allows us to represent indirectly the possible different sensitivity to treatment of cycling cells with respect to quiescent cells (at low σ values, indeed, a high fraction of quiescent cells will be present). These death rates are assumed here to depend on the *actual* values of σ and c: we will see in sections 5.2 and 5.3 a generalization of this assumption. In the necrotic region, for $r > \rho_N(t)$, the balance equations reduce to

$$\frac{\partial \nu_N}{\partial t} + \mathrm{div}(u\,\nu_N) = -\tilde{\mu}_N\nu_N\,. \tag{3}$$

Since $\nu_V(r,t)+\nu_N(r,t)$ is constant in view of assumption *(ix)*, by adding equations (1)-(2) and by (3) it is easy to obtain

$$\mathrm{div}\,u = \frac{1}{r}\frac{\partial}{\partial r}(ru) = \begin{cases} \chi(\sigma)\nu - \mu_N(1-\nu) & r_0 < r < \rho_N(t) \\ -\tilde{\mu}_N & \rho_N(t) < r < B(t)\,, \end{cases} \tag{4}$$

where $\nu(r,t)$ is defined as

$$\nu(r,t) = \nu_V(r,t)/(1-\nu_E)\,. \tag{5}$$

From Eq. (4) with $u(r_0,t) = 0$ (there is in fact no cell flux across the vessel wall), the velocity field is then obtained as

$$ru(r,t) = \begin{cases} \int_{r_0}^{r} z\,[(\chi(\sigma)+\mu_N)\nu - \mu_N]\,dz & r_0 < r \le \rho_N(t) \\ \rho_N u(\rho_N,t) - (\tilde{\mu}_N/2)(r^2 - \rho_N^2) & \rho_N(t) < r \le B(t). \end{cases} \tag{6}$$

Taking into account Eq. (4) and that $\mathrm{div}(\nu u) = \nu\mathrm{div}\,u + u\partial\nu/\partial r$, from Eq. (1) the following equation for ν can be obtained

$$\frac{\partial \nu}{\partial t} + u\frac{\partial \nu}{\partial r} = \big[(\chi(\sigma)+\mu_N)(1-\nu) - \mu(\sigma) - \mu_R(\sigma,t) - \mu_C(c,\sigma)\big]\nu\,, \quad r_0 < r < \rho_N(t)\,. \tag{7}$$

Concerning the equation for σ, diffusion is by far the dominant transport mechanism for oxygen and it occurs in a quasi-stationary regime. Thus we have:

$$\Delta\sigma = f(\sigma)\nu\,, \tag{8}$$

with the boundary conditions

$$\sigma(r_0,t) = \sigma^\star \tag{9}$$

$$\left.\frac{\partial\sigma}{\partial r}\right|_{r=\rho_N(t)} = 0\,, \tag{10}$$

where $f(\sigma)$ is the ratio (times $1-\nu_E$) between the consumption rate per unit volume of viable cells and the diffusion coefficient. At the inner boundary $r=r_0$, *i.e.* at the vessel wall, we have for simplicity prescribed the (constant) oxygen blood concentration $\sigma^\star$, although a more realistic flux condition might be imposed.

Concerning now the determination of the interface $r=\rho_N(t)$, we note preliminarily that the following inequalities must be satisfied

$$u(\rho_N(t),t) - \dot\rho_N(t) \geq 0 \tag{11}$$

$$\sigma(\rho_N(t),t) \geq \sigma_N\,, \tag{12}$$

since the necrotic material cannot be converted back to living cells, and because the assumption *(v)* forbids to have viable cells at σ values smaller than σ_N. Thus, if the cells cross the interface $\rho_N(t)$, that is if $u(\rho_N,t)-\dot\rho_N>0$, the cord boundary is defined by the condition

$$\sigma(\rho_N(t),t) = \sigma_N\,, \tag{13}$$

and the interface is a *non-material* free boundary. Otherwise, the cord boundary becomes a *material* free boundary defined by

$$\dot\rho_N = u(\rho_N(t),t)\,. \tag{14}$$

The first case occurs, for instance, in the stationary state when $\mu_R=\mu_C=0$. The switch to the latter case may happen when a sudden massive destruction of cells rapidly lowers oxygen consumption, and the interface $\rho_N(t)$ defined by (13) tends to acquire a velocity larger than $u(\rho_N(t))$. The new boundary is however subjected to the constraint (12). If, during the cord evolution, $\sigma(\rho_N(t),t)$ tends to drop below σ_N, one has to switch back to the free boundary condition (13).

The equation for $\nu(r,t)$, Eq. (7), requires an initial condition

$$\nu(r,0) = \nu_0(r)\,, \tag{15}$$

but not a boundary condition for $r=r_0$, because $u(r,t)$ vanishes for $r=r_0$, nor for $r=\rho_N(t)$ since $\rho_N(t)$ satisfies the inequality (11). According to the elliptic nature of the equation for σ, we are not allowed to prescribe $\sigma(r,0)$, but there must be compatibility between ν and σ at $t=0$.

The most natural choice is to let the system evolve from the equilibrium solution corresponding to $\mu_R=\mu_C=0$, thus we assume that at $t=0$, when the treatment starts, all the cords are at the stationary state. We will describe in the next section the steady state of the system. In this state, a radius B_0 exists where $u=0$ and, at this boundary, there is no exchange of cellular material and oxygen with the external environment. During the treatment, the equation

$$\dot B = u(B(t),t)\,, \quad B(0)=B_0 \tag{16}$$

describes the motion of the external boundary, $B(t)$, of the necrotic region. According to our idealized geometry, $2B$ represents the distance between the axes of adjacent vessels in a regular hexagonal array of cords.

To describe the effects of drug treatments, the model must be complemented with the transport equation for c. Also for the cytotoxic chemical we do not distinguish the concentrations inside and outside the cells, and we assume uniform diffusivity. Again, it can be assumed that the transport is mainly diffusive, but we do not consider the process as quasi-stationary because the drug concentration in the blood vessel may undergo rapid changes due to the administration modality and the pharmacokinetics of the drug. Some drugs have indeed fast clearance rates: for instance, 5-Fluorouracil shows a half-life in plasma of about ten minutes (Joulia *et al.*, 1997). Therefore we have for the concentration $c(r,t)$ the following diffusion-absorption equation:

$$\frac{\partial c}{\partial t} - D_C \Delta c = -\varphi_C(c,\sigma)\nu - \lambda c\,, \tag{17}$$

with

$$c(r_0,t) = c^\star(t)\,, \tag{18}$$

$$\left.\frac{\partial c}{\partial r}\right|_{r=B(t)} = 0\,, \tag{19}$$

$$c(r,0) = 0\,, \tag{20}$$

where: D_C is the diffusion coefficient of the drug, $\varphi_C(c,\sigma)$ represents the net rate of drug uptake and metabolism by the tumour cells, and the rate constant λ represents an additional loss, possibly related to a natural decay of c (if the substance is chemically unstable). The function $c^\star(t)$ in (18) will represent the pharmacokinetics of the drug in the tumour vasculature, whereas condition (19) is consistent with the reflecting nature of the boundary B. The dependence of φ_C on c takes into account the modality of uptake, whereas through the dependence on σ it is possible to insert in the model the different drug uptake by cycling and quiescent cells. We notice that the boundary condition (18) could be substituted by a flux condition. In this way, the permeability of the vessel wall to drug would be explicitly represented by an additional model parameter.

The model might be rewritten in a non-dimensional form by considering the following non-dimensional variables:

$$t' = \frac{t}{T_{d0}} \qquad r' = \frac{r}{r_0}$$

$$u' = \frac{T_{d0}}{r_0}u\,, \qquad \sigma' = \frac{\sigma}{\sigma_N}\,, \qquad c' = \frac{c}{\bar{c}}$$

where $T_{d0} = \ln 2/\chi_0$ is the doubling time of the cell population corresponding to the maximal proliferation rate, and $\bar{c}$ is a characteristic drug concentration that can be chosen among the parameters describing the action of the drug (see section 5.3). In our exposition however, except for the drug concentration, we will use the original variables for a more immediate reference to the biological meaning of the results.

4. The steady state

In the absence of treatment, we may consider the problem of the existence of a constant cord radius ρ_{N0} and a time-independent solution $\sigma(r)$, $\nu(r)$, $u(r)$ that satisfy

$$u\frac{\partial \nu}{\partial r} = \big[(\chi(\sigma)+\mu_N)(1-\nu)-\mu(\sigma)\big]\nu\,, \quad r_0<r<\rho_{N0}\,, \tag{21}$$

together with Eqs. (6), (8)-(10) and (13), with the requirement $u(\rho_{N0})>0$. For suitable values of the parameters, the existence and uniqueness of this stationary solution was proved in Bertuzzi *et al.* (submitted). A necessary condition for the existence of a finite ρ_{N0} is $f(\sigma_N)>0$. If $f(\sigma_N)$ were equal to zero, indeed, the problem (8), (10) and (13) for any finite ρ_N could only have the constant solution $\sigma\equiv\sigma_N$. Since $u(\rho_{N0})>0$, according to (6) there will exist a radius B_0, $B_0>\rho_{N0}$, such that $u(B_0)=0$.

Equation (21) is degenerate at r_0 because $u(r_0)=0$. We have then assumed $\mu(\sigma)=\mu_{min}\geq 0$ for $\sigma\geq\sigma_P$ (with $\sigma_P<\sigma^\star$) so that there exists an inner region of the cord in which both proliferation and death rates are constant. In this case, it is easy to see that the solution ν is constant and equal to

$$\nu_{max} = 1-\frac{\mu_{min}}{\chi_0+\mu_N} \tag{22}$$

for $r_0<r<\rho_P$, with the radius ρ_P such that $\sigma(\rho_P)=\sigma_P$. Taking into account Eq. (22), we can note that the condition $\chi_0>\mu_{min}$ is necessary in order to have a positive velocity field. As a matter of fact, it can be checked that $\chi_0-\mu_{min}$ is the value of the right derivative of u at r_0. Moreover, it can be proved that the volume fraction ν remains positive and decreasing in the interval $(\rho_P,\rho_N]$, unless $\mu\equiv 0$, in which case $\nu(r)=1$ in all the interval $(r_0,\rho_N]$.

Depending on the values of parameters, a different steady state may exist in which the necrotic region is absent. In that case u vanishes before σ attains the death threshold σ_N, and B_0 is defined by $u(B_0)=0$ and $\sigma_r(B_0)=0$, while in general $\sigma(B_0)>\sigma_N$. This stationary state is expected to occur when μ and μ_N are sufficiently large, so that the dead cell mass is quickly removed. Numerical computations (not shown) confirm this conjecture. A similar stationary steady state appears to occur in the dormant micrometastases observed by Holmgren *et al.* (1995), in which no necrosis is present.

The numerical solution of the steady-state problem was computed according to the procedure described in Appendix A1. In all the simulations presented in this and the following sections, the function $f(\sigma)$ has the form (Bertuzzi and Gandolfi, 2000):

$$f(\sigma) = \begin{cases} F_P\dfrac{\sigma}{K_\sigma+\sigma} & \sigma\in[\sigma_P,\sigma^\star] \\ \left[F_Q\dfrac{\sigma_P-\sigma}{\sigma_P-\sigma_Q}+F_P\dfrac{\sigma-\sigma_Q}{\sigma_P-\sigma_Q}\right]\dfrac{\sigma}{K_\sigma+\sigma} & \sigma\in[\sigma_Q,\sigma_P] \\ F_Q\dfrac{\sigma}{K_\sigma+\sigma} & \sigma\in[\sigma_N,\sigma_Q] \end{cases} \tag{23}$$

where F_P and F_Q are the maximal O_2 consumption rates of proliferating and quiescent cells, respectively, and K_σ is a Michaelis-Menten constant. The values of the parameters as well as the definition of the function $\chi(\sigma)$ are specified in the legend of Figure 2.

Figure 2 shows examples of the stationary solutions for σ, ν and u obtained for different choices of the function $\mu(\sigma)$. We note that, even in the case of $\mu(\sigma)$ constant, the viable cell

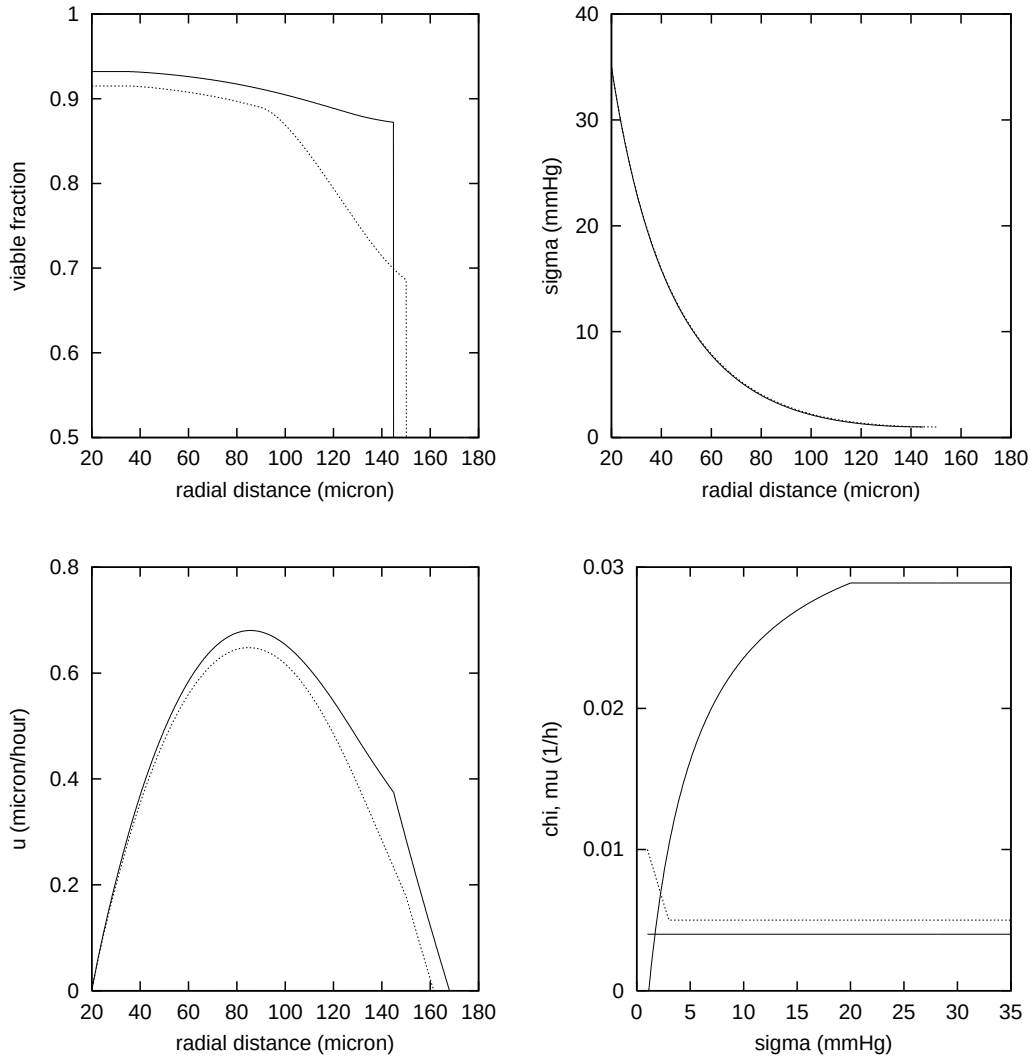

Fig. 2. Profiles of $\nu(r)$ (upper left panel), $u(r)$ (lower left) and $\sigma(r)$ (upper right) at the stationary state, and profiles of the assumed $\chi(\sigma)$ and $\mu(\sigma)$ functions (lower right). Parameter values (O_2 concentration in mmHg, length in μm, time in h): $r_0 = 20$, $\sigma^\star = 35$, $\sigma_P = 20$, $\sigma_Q = 1.125$, $\sigma_N = 1$, $\mu_N = 0.03$, $\tilde{\mu}_N = 0.015$. Moreover: $F_P = 0.016$, $F_Q = F_P/3$, $K_\sigma = 4.32$ (Casciari *et al.*, 1992); $\chi(\sigma)$ increasing as a Michaelis-Menten curve in (σ_Q, σ_P) from 0 to $\chi_0 = \ln 2/T_{d0}$, with $T_{d0} = 24$ and $\chi = \chi_0/2$ at $\sigma = (5\sigma_Q + \sigma_P)/6$. Two different functions $\mu(\sigma)$ were considered: $\mu(\sigma)$ constant and equal to 0.004 (solid lines); $\mu(\sigma)$ linearly decreasing from $\mu_{max} = 0.010$ at $\sigma = \sigma_N$ down to $\mu_{min} = 0.005$ at $\sigma = 3$ and then constant (dotted lines).

fraction is decreasing after ρ_P because of the decreasing cell proliferation rate as the radial distance increases. In Fig. 2, the radial distance where u vanishes marks the value B_0 of the external boundary B. At $r = \rho_{N0}$, it is $u > 0$ and the cord boundary is thus a non-material boundary. With the parameter values chosen, the stationary radius of the cord is in the range of the values experimentally observed. In this figure, the extent of the spontaneous cell death has been increased for illustrative purposes: experimental data reported by Moore *et al.* (1984) show necrotic fractions within the cord that do not exceed 10%.

5. The response to treatment

The numerical solution of the evolutive problem that originates from the perturbation induced by treatment has been obtained assuming the stationary state as the initial condition. The numerical procedure is briefly described in the Appendix A2. We will organize our results into three subsections: the basic features of the cord response, the incorporation of radioresistance in the model, and the response to cytotoxic drugs.

5.1. The basic response

We start considering the simplest case, that however provides a prototype of the cord response, in which only the death rate μ_R is present, and this rate is a function $\beta(t)$ of time only.

To describe the delayed effects that follow the delivery of a single dose of radiation at $t=0$, $\beta(t)$ will have the form of a broadened pulse. Although the delivery time is very short (few minutes), cell death may last indeed for many hours after irradiation, sometimes even during the lifespan of the successive cell generations (Bristow and Hill, 1998; Forrester *et al.*, 1999). In the simulations here presented, we have assumed for $\beta(t)$ a trapezoidal pattern with a rising front lasting 2 h, a plateau until 10 h, and a descending front of variable length, T being the total duration of the pulse and μ_{Rmax} the plateau value. In all the following simulations, we have taken $\mu(\sigma)=0$.

Figure 3 (upper panel) shows the geometrical variables of the cord. As indicated by the time evolution of $\sigma(\rho_N(t),t)$ (lower left panel), the cord boundary ρ_N, which is non-material at the stationary state, quickly turns into a material interface and so it remains during all the regression phase, confirming the crucial role of the constraints (11)-(12) in the model. Then, the boundary switches again to be non-material during the regrowth phase with a slope discontinuity. The figure also shows the behaviour of $B(t)$, and of the radii $\rho_P(t)$ and $\rho_Q(t)$ where the oxygen tension has the values σ_P and σ_Q respectively. The time course of these latter radii, together with that of $\sigma(\rho_N)$ in the lower left panel, reveals a substantial reoxygenation of the cord for a long period after the treatment. We recall that in the region between r_0 and ρ_P the proliferation rate is maximal, whereas between ρ_Q and ρ_N all cells are quiescent. The lower right panel of Fig. 3 represents the ratio between the total volume (per unit cord length) of viable cells and its value at $t=0$, that is $\int_{r_0}^{\rho_N(t)} r\nu(r,t)\,dr / \int_{r_0}^{\rho_{N0}} r\nu(r,0)\,dr$. The strong increase of μ_R causes a marked depletion of viable cells during the interval $[0,T]$. Whereas the minimum of viable cell number occurs at $t=T$, the minima of ρ_N and B occur later, this fact being related to the non-instantaneous degradation of dead cells.

The effect of changes in the degradation rate of dead cells is shown in Fig. 4. As expected from the expression of the cell velocity, the cord regression (and the regression of B) are more pronounced when the degradation rates are increased. The occurrence time of the minimum of ρ_N does not appear to be substantially changed in this simulation, however a faster response can be obtained by larger values of μ_N. Figure 5 shows the effects of treatments with different $\beta(t)$ patterns. First, we have considered patterns with the same area, from a very broadened pulse to a sharp one. In particular, we assumed $\beta(t)=k\tilde{\beta}(kt)$ where $\tilde{\beta}(t)$ has the trapezoidal shape previously described, with $\mu_{Rmax}=0.24\,\mathrm{h}^{-1}$ and $T=12\,\mathrm{h}$. As we can see, when the death rate approaches an impulse, the cord response appears to converge to a limit behaviour in which the minimum of the regression is reached after some irreducible time. Then, we have considered patterns with reduced area: an unexpected behaviour occurs in response to low intensity treatments, that lead to a slight increment of the cord radius. This response can

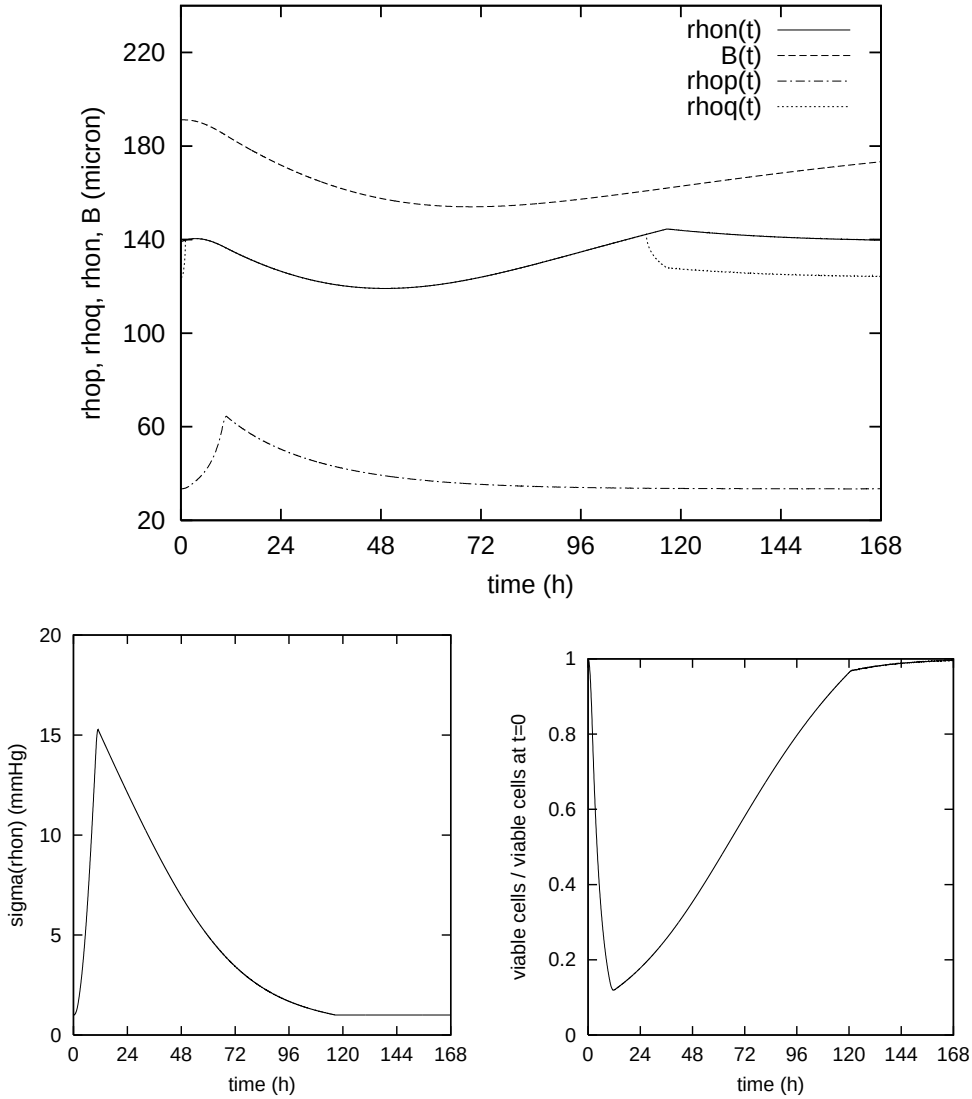

Fig. 3. Basic response: time course of the geometrical variables of the cord (upper panel), of the oxygen concentration at the cord boundary (lower left panel) and of the normalized total fraction of viable cells (lower right panel). Model parameters as in Fig. 2, except $\mu(\sigma) = 0$, $\mu_N = 0.02$, $\tilde{\mu}_N = 0.01$. Parameters of the treatment: $\mu_{Rmax} = 0.24\,\mathrm{h}^{-1}$, $T = 12$ h.

be explained by considering that a moderate cell death with a small reduction in ν may be unable to produce the inversion of the velocity at $r = \rho_N$; on the other hand, the reduced oxygen consumption does allow cell viability at values of ρ_N larger than the stationary value. Of course, as expected, also in these cases the total volume of viable cells initially decreases (not shown). An instance of moderate expansion of the cord radius after the treatment appears to occur in data reported by Moore *et al.* (1983).

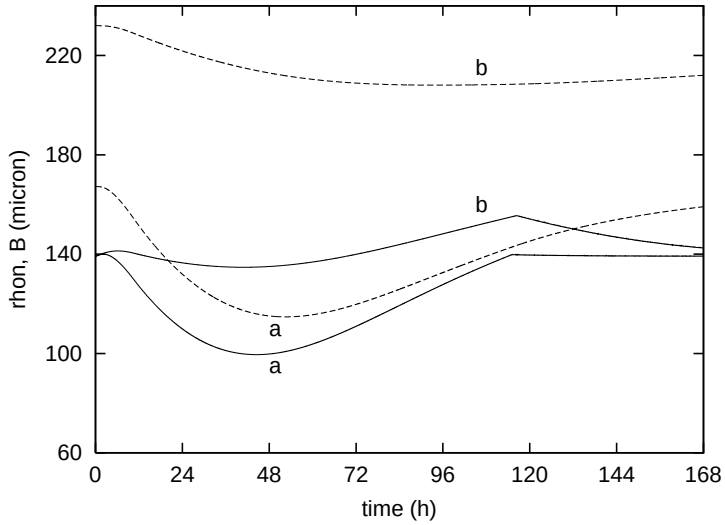

Fig. 4. Effect of changes in the degradation rate of dead cells: $\rho_N(t)$ (solid lines), $B(t)$ (dashed lines). (a) $\mu_N = 0.04$, $\tilde{\mu}_N = 0.02$; (b) $\mu_N = 0.01$, $\tilde{\mu}_N = 0.005$. Other parameters as in Fig. 3.

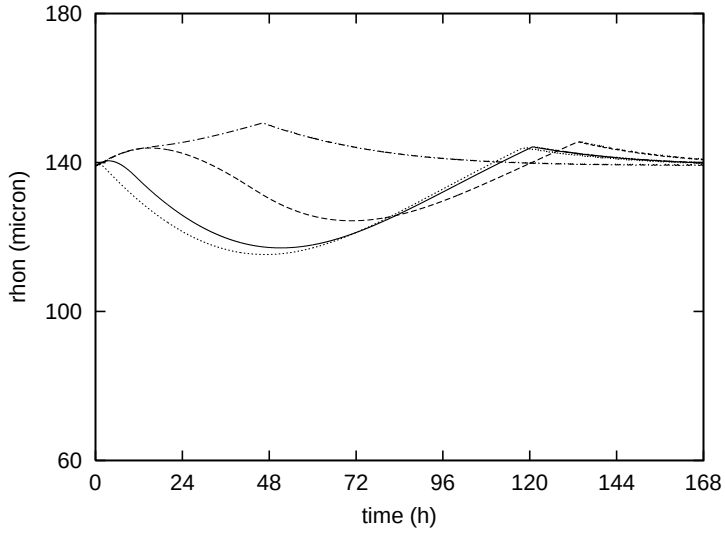

Fig. 5. Effect on the cord radius of changes in $\beta(t)$. Patterns with the same area: $k = 0.25$ (dashed), $k = 1$ (solid), $k = 4$ (dotted). Pattern with reduced area: $\mu_{Rmax} = 0.04\,\mathrm{h}^{-1}$, $T = 20\,\mathrm{h}$ (dash-dotted). Other parameters as in Fig. 3.

5.2. Radioresistance

It is well known that the effects of radiation are influenced by the oxygenation status of the cells: hypoxic cells are less sensitive than well-oxygenated cells (see, *e.g.*, Bristow and Hill, 1998).

To account for the dependence of the rate of cell death due to radiation on the oxygenation status, two extreme hypotheses may be considered: (I) The death rate at a certain time t and radial distance r, that we denote as $\tilde{\mu}_R(r,t)$, depends on the oxygen concentration at (r,t):

$$\tilde{\mu}_R(r,t) = \mu_R(\sigma(r,t),t)\,. \tag{24}$$

This hypothesis has been incorporated in the formulation of the model as described in section 3. (II) The death rate of a cell, that at time t is at the radial distance r, depends on the oxygen concentration that the cell or its ancestors had experienced at the time of delivery of the radiation pulse. In this case we write:

$$\tilde{\mu}_R(r,t) = \mu_R(\sigma(\zeta(r,t),0),t)\,, \tag{25}$$

where $\zeta(r,t)$ is the initial position of a cell which is in (r,t). Thus ζ is such that

$$\eta(\zeta(r,t),t) = r\,, \tag{26}$$

$\eta(\hat{r},t)$ being the trajectory starting from $\hat{r}$ at $t=0$ as defined by the following equation:

$$\dot{\eta} = u(\eta,t)\,, \qquad \eta(\hat{r},0) = \hat{r}\,. \tag{27}$$

In the case (II), the numerical solution of the corresponding evolutive problem can be obtained by means of simple changes in the scheme described in the Appendix.

We make the further assumption that, in both cases, the rate of cell death due to radiation is the product of a function of time, $\beta(t)$, and a function of σ, $\psi_R(\sigma)$. In view of the results obtained by Chapman *et al.* (1974) on survival curves, we have chosen

$$\psi_R(\sigma) = \frac{1}{3}\left(1 + 2\frac{\sigma - \sigma_N}{2.0 + \sigma - \sigma_N}\right), \tag{28}$$

(with σ expressed in mmHg) so that the radiosensitivity of a hypoxic cell is around 1/3 the radiosensitivity of a well-oxygenated cell.

The two hypotheses on the modality of radioresistance are compared in Fig. 6. The upper panel shows that the cord regression is less pronounced in the case (II), indicating a more effective radioresistance. On the contrary, under hypothesis (I), the rapid reoxygenation of cells makes the cells sensitive to radiation (as long as $\beta > 0$) even at the cord periphery. This increased sensitivity is confirmed by the lower panel, that depicts the profiles of ν as a function of r at various times, showing the larger depletion of viable cells in the entire cord.

The importance of modelling the dynamics of oxygen concentration, and of accurately representing the differences in radiosensitivity related to oxygenation, is highlighted by comparing the effect of a single dose against two equal fractions delivered 24 h apart. Figure 7 shows this comparison in terms of the fraction of total viable cells. More precisely, we have considered a death rate $\beta(t)$ (plots denoted by "a" in the figure), and a death rate given by $0.5\beta(t)+0.5\beta(t-24)$ (plots denoted by "b"). When the cell death rate is independent of oxygen concentration, the dose splitting does not improve the response, as expected in view of the cell repopulation that occurs between the two pulses. On the contrary, having assumed the radioresistance of hypoxic cells (according to modality II), the fractionated treatment produces an increased cell killing. In this case, in fact, the second pulse finds the cell population in a markedly reoxygenated condition.

We conclude this subsection by showing the model fitting of two experimental responses of cord radius to a single dose of radiation that are reported in the literature (Fig. 8). The data reported by Tannock and Howes (1973) refer to tumour cords in a C3H mouse mammary adenocarcinoma implanted in mice (dose: 6 Gy), whereas the data in Moore *et al.* (1983) refer to the rat Morris hepatoma 3924A implanted in rats (dose: 15 Gy). The radius of the central vessel

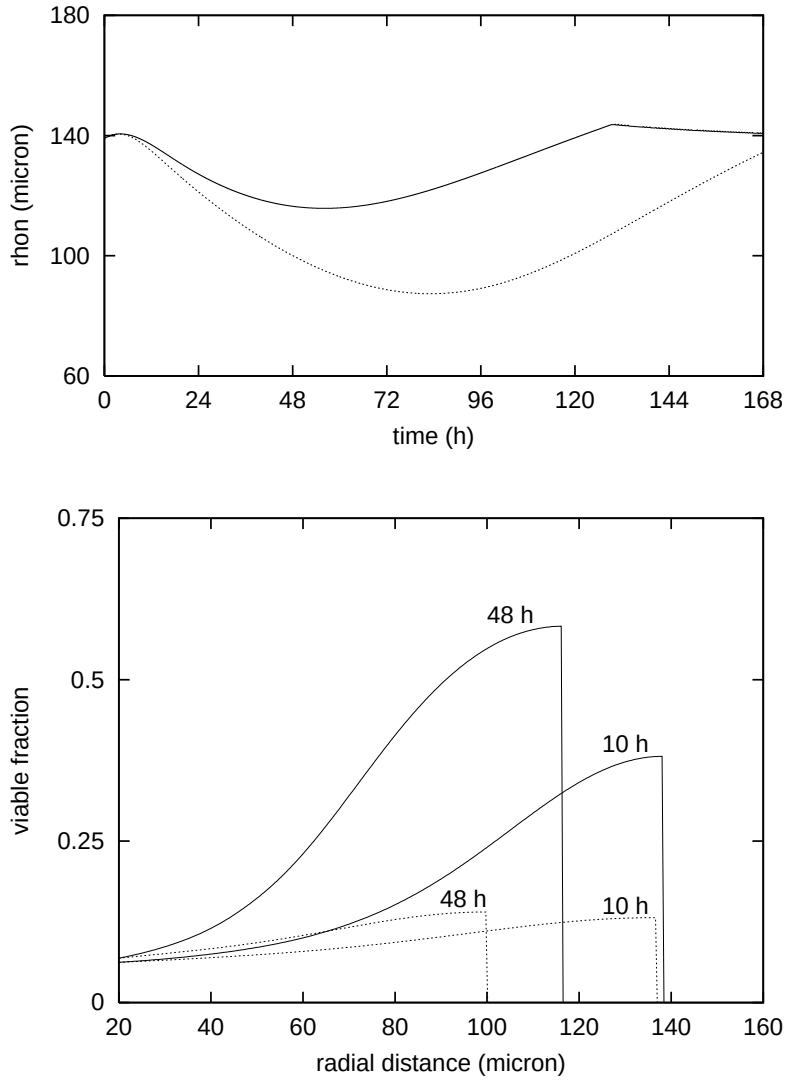

Fig. 6. Comparison between two different modalities of oxygen-related radioresistance. Time course of cord radius (upper panel); profiles of ν at the times indicated (lower panel). Modality (I), dotted lines; modality (II), solid lines. Other parameters as in Fig. 3.

was set at the value of 20 μm for the Morris hepatoma, as reported in Moore *et al.* (1983), and at 10 μm for the C3H tumour according to the value measured in a similar tumour (Tannock, 1968). For obtaining a stationary cord radius equal to the experimental values in the untreated cords, different values of $\sigma^\star$ were assumed for the two tumours (see the legend of Fig. 8). The model fitting was obtained by a trial-and-error procedure, representing the radioresistance of hypoxic cells in both tumours according to the modality II described above. The dynamics of the response is markedly different in the two cases, the response of the C3H tumour cords being much faster, so that the parameter values of the fitting curves were very different. In particular, for the C3H tumour cord, we assumed: a short T_{d0} value (equal to 14 h, as reported for a similar tumour by Tannock (1968)), a rapid degradation of dead cells, and a pattern of $\beta(t)$ with high intensity and a very short duration ($\beta(t)$ increasing from 0 up to 4.5 h^{-1} at 0.5 h, then constant up to 1 h, and finally decreasing to 0 at 1.5 h). For the 3924A cord, instead, it

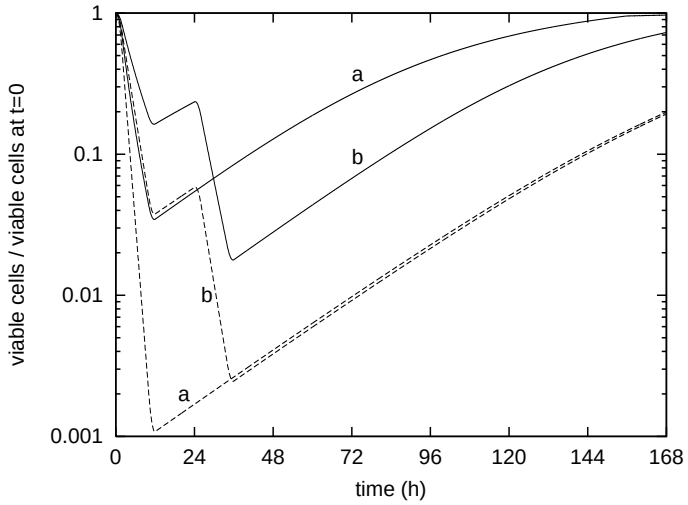

Fig. 7. Total viable cells after a single dose (a) or a two-fractions treatment (b). Cell death rate independent of O_2 concentration (dashed lines); death rate dependent on O_2 concentration (solid lines). Single pulse: $\mu_{Rmax} = 0.72\,\mathrm{h}^{-1}$, $T = 12\,\mathrm{h}$; the two pulses have half intensity and start 24 h apart. Other parameters as in Fig. 3.

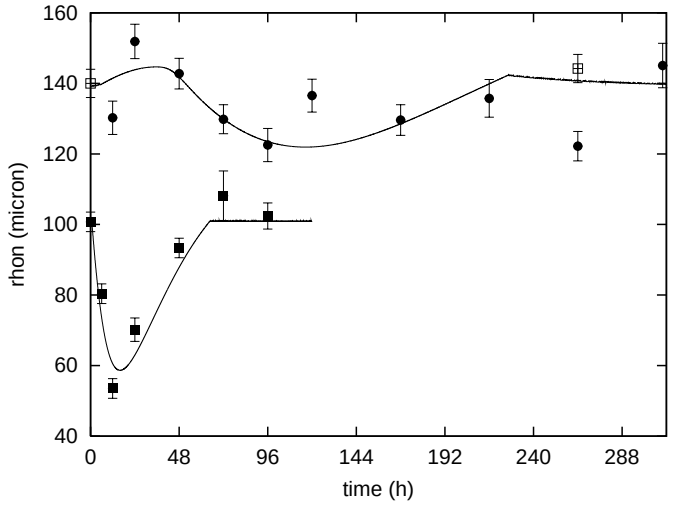

Fig. 8. Experimental data of cord radius after a single dose of radiation and model predictions. Data replotted from Tannock and Howes (1973): closed squares. Parameter values (concentration in mmHg, length in μm, time in h): $r_0 = 10$, $\sigma^\star = 19$, $\sigma_P = 13$, $T_{d0} = 14$, $\mu_N = 0.166$, $\beta(t)$ as described in the text. Data from Moore *et al.* (1983): closed circles (untreated controls, open squares). Parameter values: $r_0 = 20$, $\sigma^\star = 35$, $\sigma_P = 20$, $T_{d0} = 48$, $\mu_N = 0.015$, $\beta(t)$ as described in the text. Other parameters as in Fig. 3 with $\mu(\sigma) = 0$.

was necessary to assume a larger T_{d0} of 48 h, a slow degradation rate, and a very prolonged duration of β. Moreover, the pattern of β needed to have a long initial tract with low intensity ($\beta(t)$ increasing from 0 to $0.04\,\mathrm{h}^{-1}$ at 36 h, then increasing from $0.04\,\mathrm{h}^{-1}$ to $0.24\,\mathrm{h}^{-1}$ at 44 h, and finally decreasing to 0 at 56 h): this initial delay could be related to the occurrence of cell death mainly in the generations successive to the irradiated generation (Forrester *et al.*, 1999). We notice that the T_{d0} value used for this cord exceeds the experimental value of the cell cycle time

(27.4 h) reported in Moore *et al.* (1984). This discrepancy might be interpreted by considering that the T_{d0} value used in our fitting might mimic the possible cytostatic effects of the radiation.

5.3. The response to cytotoxic drugs

Anticancer drugs are known to produce a complex pattern of effects on tumour cells (Boyer and Tannock, 1998). *In vitro* experiments in which tumour cells were exposed to drugs for a short period, showed either blocks of cell cycle progression in different cell cycle phases and cell death, both these effects extending far beyond the incubation time (Montalenti *et al.*, 1998; Sena *et al.*, 1999).

Even when restricting to cytotoxic effects, it is not simple to assess the relation between drug concentration and cell death. We will assume that the cell death rate μ_C depends on the uptake and metabolism (consumption) of drug by the cells, and that the effects of even infinitesimal consumptions cumulate linearly in time through a stationary weighting function $H(\theta)$. $H(\theta)$ is defined as the death rate induced after a time interval θ by the impulsive consumption of a unit amount of drug in the unit volume. In addition, the dependence of the drug effect on the proliferative status of the cell is indirectly accounted for by a multiplicative factor which is a function of oxygen concentration. For simplicity, we will disregard the possible dependence on σ of the rate of drug consumption φ_C.

Proceeding similarly as in the previous section, we distinguish the case in which the cell death at (r,t) depends on the oxygen concentration at (r,t), from the case in which the effect of the drug taken up at a time that precedes t depends on the oxygen concentration at that time. Thus we can write in the first and, respectively, in the second case:

$$\tilde{\mu}_C(r,t) = \int_0^t H(t-\tau)\psi_C(\sigma(r,t))\varphi_C(\hat{c}(\tau;r,t))\,d\tau \tag{29}$$

$$\tilde{\mu}_C(r,t) = \int_0^t H(t-\tau)\psi_C(\hat{\sigma}(\tau;r,t))\varphi_C(\hat{c}(\tau;r,t))\,d\tau\,, \tag{30}$$

with

$$\hat{\sigma}(\tau;r,t) = \sigma(\eta(\zeta(r,t),\tau),\tau) \tag{31}$$

$$\hat{c}(\tau;r,t) = c(\eta(\zeta(r,t),\tau),\tau)\,, \tag{32}$$

where $\psi_C(\sigma)$ $(\psi_C(\sigma) \leq 1)$ represents the reduction of the effect in relation to the oxygenation level.

In this paper, we will limit ourselves to consider the case in which the impulsive response H has a decay fast enough with respect to the dynamics of drug concentration. Under this assumption, Eqs. (29) and (30) are well approximated by the expression

$$\tilde{\mu}_C(r,t) = \mu_C(c,\sigma) = \bar{\mu}_C\psi_C(\sigma(r,t))\varphi_C(c(r,t)) \tag{33}$$

where $\bar{\mu}_C$ denotes the integral of $H(t)$. Further, we assume

$$\varphi_C(c) = \Phi_M\frac{c}{K_C + c}\,, \tag{34}$$

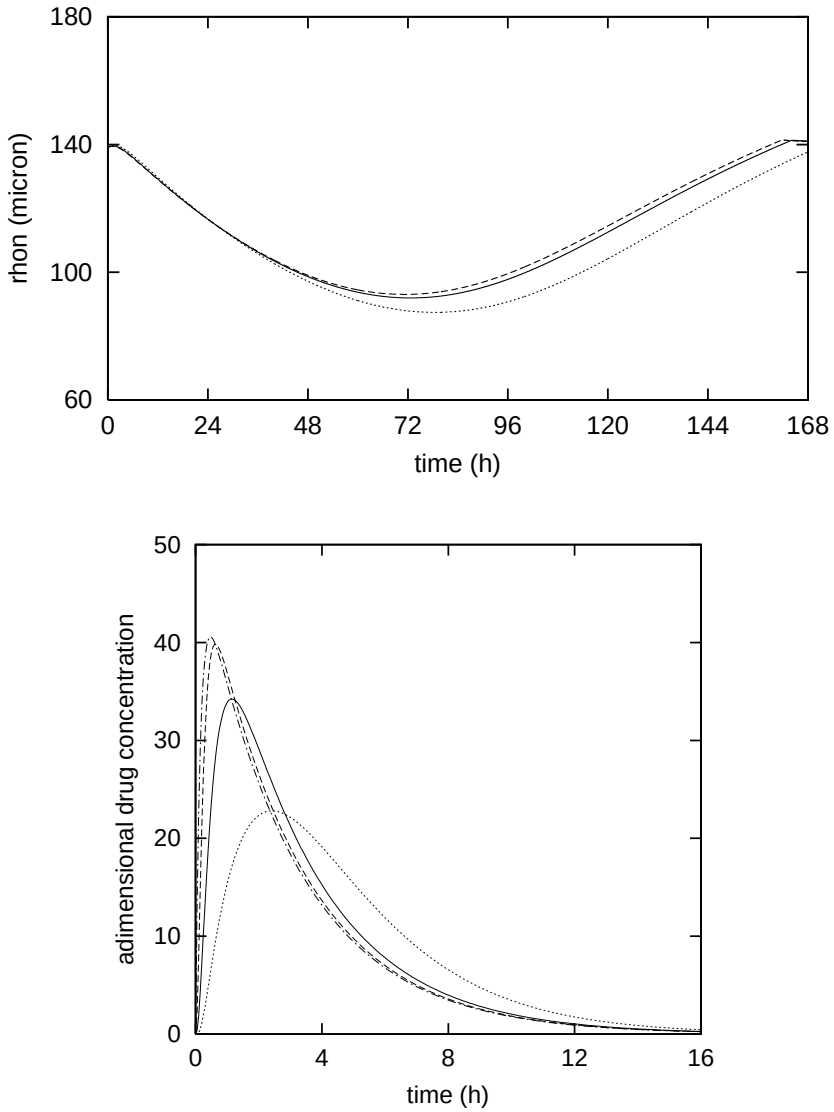

Fig. 9. Cord response to a single dose of cytotoxic drug. Effect of changes in the drug diffusion coefficient: $\rho_N(t)$ (upper panel) and non-dimensional drug concentration c' at the boundary ρ_N (lower panel). $D_C = 5\times10^{-8}$ (dotted), $D_C = 2\times10^{-7}$ (solid), $D_C = 8\times10^{-7}\,\mathrm{cm^2/s}$ (dashed). $\Phi'_M = 1.0\,\mathrm{h^{-1}}$, $K'_C = 20$, $C' = 50$, $\tau_1 = 3\,\mathrm{h}$, $\tau_2 = 0.15\,\mathrm{h}$. Other parameters as in Fig. 3. In the lower panel $c^{\star\prime}(t)$ is also shown (dash-dotted).

where Φ_M is the maximal rate of cellular uptake and metabolism, and K_C a Michaelis-Menten constant. The function $\psi_C(\sigma)$ may be expressed as

$$\psi_C(\sigma) = \begin{cases} \alpha_1 & \sigma \in [\sigma_P, \sigma^\star] \\ \alpha_2 + (\alpha_1 - \alpha_2)\dfrac{\sigma - \sigma_Q}{\sigma_P - \sigma_Q} & \sigma \in [\sigma_Q, \sigma_P] \\ \alpha_2 & \sigma \in [\sigma_N, \sigma_Q] \end{cases} \tag{35}$$

with α_1,$\alpha_2 \leq 1$. Although most drugs are less effective on quiescent cells (in this case $\alpha_1 = 1$ and $\alpha_2 < 1$), some recently developed drugs, such as tirapazamine (Brown and Siim, 1996), are selectively cytotoxic to hypoxic cells (in this case, $\alpha_1 < 1$ and $\alpha_2 = 1$).

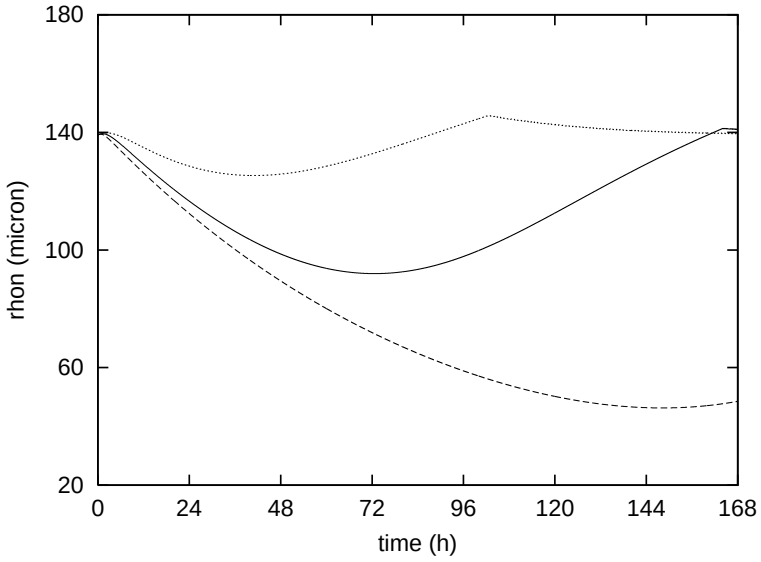

Fig. 10. Effect of changes in the maximal rate of drug consumption. $\Phi'_M = 0.5$ (dotted), $\Phi'_M = 1.0$ (solid), $\Phi'_M = 2.0\,\mathrm{h}^{-1}$ (dashed). Other parameters as in Fig. 9, with $D_C = 2\times10^{-7}\,\mathrm{cm}^2/\mathrm{s}$.

Since the specific sensitivity, $\bar{\mu}_C$, of tumour cells to a drug and the drug concentration in tumour vessels are difficult to assess, it is convenient to introduce the non-dimensional drug concentration $c' = \bar{\mu}_C c$. In this way, the diffusion-absorption equation (17) reads as follows:

$$\frac{\partial c'}{\partial t} - D_C \Delta c' = -\Phi'_M \frac{c'}{K'_C + c'}\nu - \lambda c' \,, \tag{36}$$

with

$$c'(r_0, t) = c^{\star\prime}(t) \,, \tag{37}$$

$$\left.\frac{\partial c'}{\partial r}\right|_{r=B(t)} = 0 \,, \tag{38}$$

$$c'(r, 0) = 0 \,, \tag{39}$$

where Φ'_M, K'_C, $c^{\star\prime}(t)$ denote, respectively, Φ_M, K_C, $c^\star(t)$ times $\bar{\mu}_C$. Moreover, equations (33) and (34) give

$$\mu_C(c', \sigma) = \Phi'_M \frac{c'}{K'_C + c'} \psi_C(\sigma(r, t)) \,. \tag{40}$$

In the simulations here presented, the time course $c^{\star\prime}(t)$ of the drug concentration in a tumour vessel, following the injection of a single dose, is represented as $c^{\star\prime}(t) = C'[\exp(-t/\tau_1) - \exp(-t/\tau_2)]$.

We focussed on the effects of changes in the parameters D_C, Φ'_M and K'_C. To give a greater emphasis to these effects, we have taken $\lambda = 0$ and, initially, $\psi_C = 1$. Figure 9 depicts the response of cord radius when the diffusion coefficient undergoes changes from 5×10^{-8} to 8×10^{-7} cm^2/s. These values appear to be reasonable for some commonly used drugs: for instance, the diffusion coefficient for tirapazamine is 7.0×10^{-7} cm^2/s (Kyle and Minchinton, 1999). The predicted responses shown in the figure are quite similar but, in this simulation, the decrease of D_C leads to a slight increase of cord regression. This fact can be explained by observing that the Michaelis-Menten form of the death rate unfavours the higher but shorter concentration peak

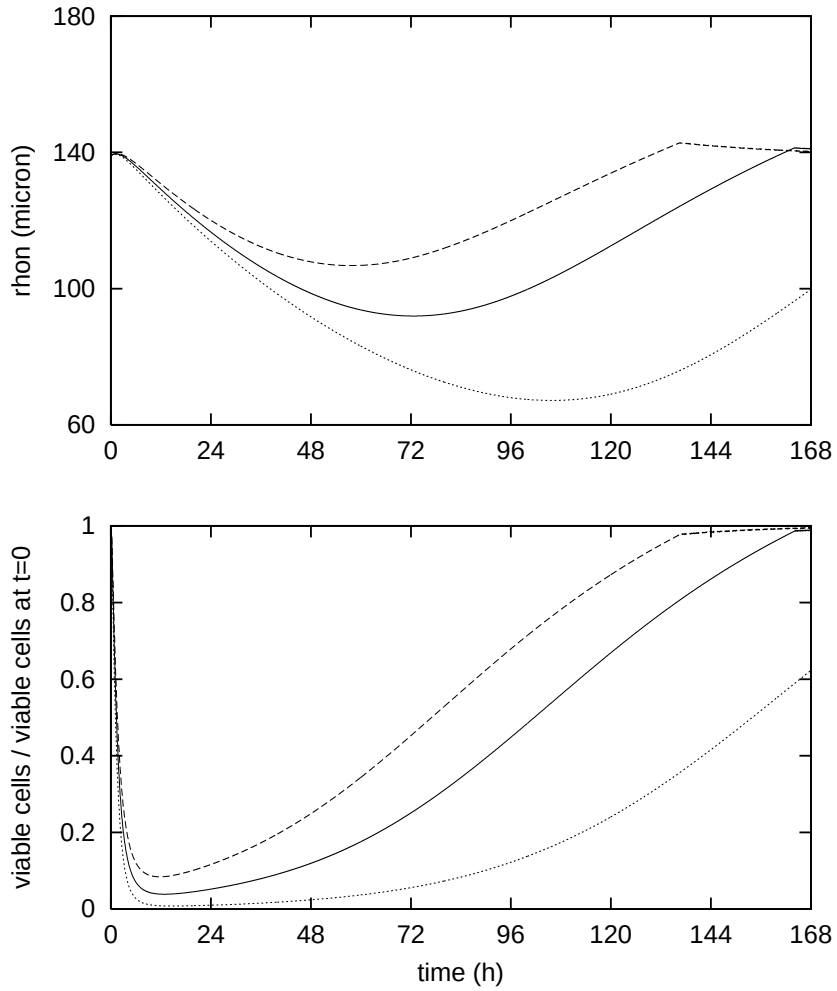

Fig. 11. Effect of changes in the Michaelis-Menten constant of drug consumption: $\rho_N(t)$ (upper panel) and normalized total fraction of viable cells (lower panel). $K'_C = 10$ (dotted), $K'_C = 20$ (solid), $K'_C = 30$. Other parameters as in Fig. 9, with $D_C = 2 \times 10^{-7}\,\mathrm{cm}^2/\mathrm{s}$.

achieved with the higher values of D_C (see the lower panel of the figure, where $c^{\star\prime}(t)$ and the drug concentration at ρ_N for the three values of D_C are reported). Much more marked changes were obtained by varying Φ'_M and K'_C (see Figs. 10 and 11).

Figure 12 compares the effect of a reduced sensitivity of hypoxic (quiescent or slowly proliferating) cells with the effect of a reduced sensitivity of well-oxygenated (rapidly proliferating) cells: the different sensitivity patterns correspond to different values of α_1 and α_2 in $\psi_C(\sigma)$. Although many factors may influence these different responses, the weaker response obtained in the present example by sparing hypoxic cells can be related to the greater initial fraction of cells in the cord region (ρ_Q, ρ_N) with respect to that in the region (r_0, ρ_P).

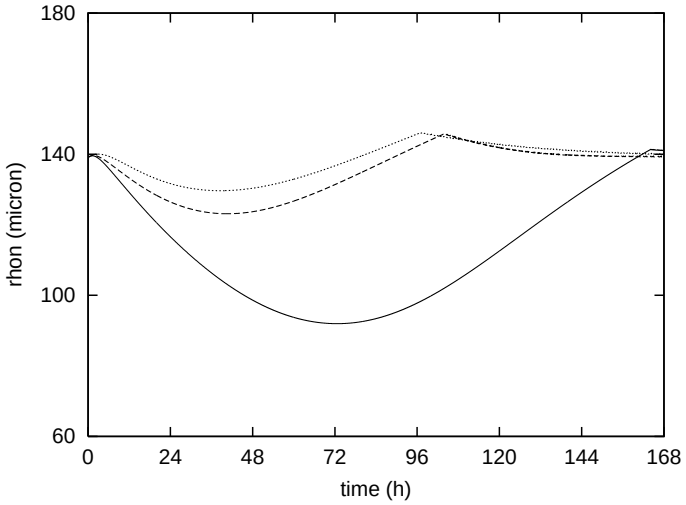

Fig. 12. Comparison among different sensitivities of cells to oxygen level. $\alpha_1 = \alpha_2$ (solid); $\alpha_1 = 1$, $\alpha_2 = 0.2$ (dotted); $\alpha_1 = 0.2$, $\alpha_2 = 1$ (dashed). Other parameters as in Fig. 9, with $D_C = 2 \times 10^{-7}\,\mathrm{cm}^2/\mathrm{s}$.

6. Concluding remarks

The model illustrated in the present paper, despite the numerous simplifying assumptions and idealizations, appears able to capture the main features of the cord response to single-dose treatments, *i.e.* the regression of the cord radius followed by regrowth towards the size observed in the untreated tumour. The continous-medium approach here adopted was able to describe substantially the experimental data considered, even though the cell size is comparable in the tumour cords to the spatial scale.

The simulations of the model have pointed out, in the regression phase of the cord, a time delay of the minimum of the cord volume with respect to the minimum of the number of tumour viable cells. This fact emphasizes the difference between the response in terms of cell viability and in terms of tumour volume, and the role of factors such as the degradation rate of dead cells in affecting the macroscopic response of the tumour mass.

A particular and valuable feature of the model is the inclusion of the oxygen concentration within the tumour cord as a model variable. This fact allowed to describe the reoxygenation process of tumour cells that follows the treatment. Thus, of the four factors that are commonly recognized as relevant in radiotherapy (the 4 R's: repair of damage, repopulation, reoxygenation, redistribution among the cycle phases after phase-specific cell death) the present model explicitly accounts for two of them, *i.e.*, cell repopulation and reoxygenation. Moreover, reoxygenation can be related to the recruitment of cells from quiescence to proliferation, and thus can be relevant in predicting the effects of drugs.

The response predicted by the model appears to be very sensitive to the mode of action of the cell killing agent, thus indicating that a more accurate description of these modalities is needed for obtaining better predictions. To this end, a model of the cell population that includes the structure of the cell cycle might be required: in such a way, the complex pattern of cytostatic and cell-killing effects that characterize the cellular response to radiation and drugs would be more completely addressed. A finer description of the response would also require the consideration of the non-istantaneous transition from cell quiescence to proliferation that is observed after changes in cell microenvironment. Moreover, the model could be usefully refined by a more

detailed representation of factors limiting the effective drug penetration in tumour tissues (Jain, 1999; Tannock, 2001).

A critical assumption of the present model is the invariance of the volume fraction occupied by viable and dead cells. Although this assumption appears to be reasonable in the untreated cord on the basis of experimental observations (Moore *et. al.*, 1983), it is likely that the fraction of extracellular fluid be different in the cord and in the necrotic region and be subjected to changes during treatments inducing cell death. Relaxing this assumption leads to the necessity of considering the full dynamics of the system, including the flow of the interstitial fluid and of the waste products. This improved model would provide both a more realistic representation of cord and tumour mass evolution, and a more correct representation of the transport of drugs for which diffusion does not dominate convection.

Appendix A: Numerical methods

We give here a short description of the numerical procedure used to compute the stationary solution and the solution of the evolutive problem.

A.1. Stationary solution

The numerical solution of the steady-state problem was obtained through an iterative procedure whose steps are described as follows:

1) $\sigma(r)$, ρ_N (and ρ_P) are initially determined assuming $\nu(r)=\nu_{max}$, with ν_{max} given by Eq, (22), by means of a shooting procedure that adjusts ρ_N to obtain $\sigma(r_0)=\sigma^\star$. The radius ρ_N is found by the bisection method in the interval from r_0 to a suitably assigned value. For each current value of ρ_N, Eq. (8) is solved numerically backward from ρ_N, imposing $\sigma(\rho_N)=\sigma_N$ and $\sigma_r(\rho_N)=0$.
2) $\nu(r)$ is obtained by integrating Eq. (21) by the Euler method, starting from ρ_P and using the current determination of $\sigma(r)$ and ρ_N. In Eq. (21), u is given by Eq. (6) and is computed by the trapezoidal rule. ν is computed, after setting σ to σ_N for $r>\rho_N$, beyond ρ_N and up to a radius r_{max} such that $u(r_{max})=\varepsilon$, $\varepsilon>0$ suitably small.
3) $\sigma(r)$, ρ_N (and ρ_P) are determined as in step 1), using the $\nu(r)$ function found in the preceding step. More precisely, the required $\nu(r)$ values are computed by linear interpolation of the values obtained in the preceding step. For the shooting, the bisection is performed in the interval $[r_0, r_{max}]$.

The steps 2)–3) are repeated until an acceptable convergence of the functions $\sigma(r)$ and $\nu(r)$ is achieved. With reasonable values of the parameters, 10-12 iterations were sufficient to stabilize the solution.

A.2. Solution of the evolutive problem

The basic feature of the procedure is to compute the viable cell fraction ν along a prefixed set of characteristic lines of Eq. (7). Let us denote by $\eta(\hat{r}, t)$ the characteristic line given by

$$\dot{\eta} = u(\eta, t)\,, \qquad \eta(\hat{r}, 0) = \hat{r}\,. \tag{A1}$$

Let δt be the time step, and $\mathcal{M}$ a given set of equispaced starting points $\hat{r}$ in $[r_0, B_0]$. Supposing to have the solution ν, u, σ and c at time t:

1) for each $\hat{r}$ in $\mathcal{M}$, we compute the characteristic line at $t+\delta t$ by the Euler formula using the velocity u at time t; then we compute the value of ν at $t+\delta t$ along the line according to Eq. (7) using the values $\sigma(\eta(\hat{r},t),t)$, $c(\eta(\hat{r},t),t)$ and $\nu(\eta(\hat{r},t),t)$;
2) the characteristic line passing through $(\rho_N(t),t)$ is also computed at $t+\delta t$. From this value, denoted as $\bar{r}$, the equation (8) for σ is solved backward on $[r_0,\bar{r}]$ with $\sigma(\bar{r})=\sigma_N$ and $\sigma_r(\bar{r})=0$. In this computation the variable transformation $x=\log r$ is used. The transformation simplifies the Laplacian to a second-order derivative (Smith, 1965), and in our problem assigns a finer grid where the solution is more rapidly changing. Let $\bar{\sigma}(r)$ be the solution. If:

(a) $\bar{\sigma}(r_0)\geq\sigma^\star$, we search the value $\rho_N(t+\delta t)$ as the value such that the function σ, satisfying Eq. (8) with $\sigma(\rho_N)=\sigma_N$ and $\sigma_r(\rho_N)=0$ reaches $\sigma^\star$ at $r=r_0$. Then we take the resulting function σ as $\sigma(\cdot,t+\delta t)$;

(b) $\bar{\sigma}(r_0)<\sigma^\star$, we set $\rho_N(t+\delta t)$ to $\bar{r}$ and the function σ at $t+\delta t$ is computed by searching the value of $\sigma(\bar{r})$ that gives $\sigma^\star$ at r_0, solving (8) backward with $\sigma_r(\bar{r})=0$;
3) the velocity field at $t+\delta t$ is computed on the basis of Eq. (6) at the points $\eta(\hat{r},t+\delta t)$ and at $\rho_N(t+\delta t)$;
4) c at $t+\delta t$ is computed solving Eq. (17) with the boundary conditions (18)-(19) by the Crank-Nicolson method.
Since the spatial grids for the variables ν, σ and c are different (and are changing with the time), suitable interpolations are performed to have these three variables at the same r values.

We give here some further details on the application of the Crank-Nicolson method (Smith, 1965) to our problem. After the variable transformation $x=\log r$ and still using c to denote concentration as function of x, Eq. (17) can be rewritten as

$$\frac{\partial c}{\partial t}=\mathrm{e}^{-2x}D_C\frac{\partial^2 c}{\partial x^2}-\varphi_C(c(x,t))\nu(x,t)-\lambda c(x,t)\,. \tag{A2}$$

Let us divide the interval $[\log r_0,\log B(t+\delta t)]$ in M equal parts, being $\delta x=(\log B-\log r_0)/M$. Let $x_i=\log r_0+(i-1)\delta x$, $i=1,\cdots,M+1$, be the generic grid point. Moreover, we denote $c_i=c(x_i,t+\delta t)$, $\hat{c}_i=c(x_i,t)$ and $\nu_i=\nu(x_i,t+\delta t)$, $\hat{\nu}_i=\nu(x_i,t)$, the $\hat{c}_i$'s and $\hat{\nu}_i$'s being obtained by linear interpolation from the values computed on the grid at time t. Then we can write, for $i=2,\cdots,M$,

$$\begin{aligned}\frac{c_i-\hat{c}_i}{\delta t}=\frac{1}{2}\Bigg[&\mathrm{e}^{-2x_i}D_C\frac{c_{i+1}-2c_i+c_{i-1}}{\delta x^2}-\varphi_C(c_i)\nu_i-\lambda c_i\\&+\mathrm{e}^{-2x_i}D_C\frac{\hat{c}_{i+1}-2\hat{c}_i+\hat{c}_{i-1}}{\delta x^2}-\varphi_C(\hat{c}_i)\hat{\nu}_i-\lambda\hat{c}_i\Bigg]\,.\end{aligned} \tag{A3}$$

Since $\varphi_C(c)$ is a nonlinear function, we perform the linearization:

$$\varphi_C(c_i)=\varphi_C(\hat{c}_i)+\left.\frac{d\varphi_C}{dc}\right|_{\hat{c}_i}(c_i-\hat{c}_i)\,. \tag{A4}$$

Thus, after some algebra, we obtain the following system of linear equations

$$\begin{aligned}a_2c_2+c_3&=b_2-c^\star(t+\delta t)\\c_{i-1}+a_ic_i+c_{i+1}&=b_i\,,\qquad i=3,\cdots,M-1\\c_{M-1}+(a_M+1)c_M&=b_M\,,\end{aligned} \tag{A5}$$

where the a_i's and b_i's are known quantities and the boundary conditions (18) and (19) are taken into account. The diagonally dominant tridiagonal system (A5) is solved by the Gauss elimination method, and c_{M+1} is set equal to c_M.

References

1. J.A. Adam and S.A. Maggelakis (1990) Diffusion regulated growth characteristics of a spherical prevascular carcinoma. *Bull. Math. Biol.* **52**, 549-582.

2. D. Ambrosi and L. Preziosi (2002) On the closure of mass balance models for tumour growth. *Math. Models Methods Appl. Sci.* **12**, 737-754.

3. A. Bertuzzi and A. Gandolfi (2000) Cell kinetics in a tumour cord. *J. theor. Biol.* **204**, 587-599.

4. A. Bertuzzi, A. Fasano and A. Gandolfi (2000) A mathematical model for the growth of tumor cords incorporating the dynamics of a nutrient. In *Free Boundary Problems: Theory and Applications II* (N. Kenmochi, Ed.), Math. Sci. Appl. 14, Gakkotosho, Tokyo, pp. 31-46.

5. A. Bertuzzi, A. Fasano, A. Gandolfi and D. Marangi (2002) Cell kinetics in tumour cords studied by a model with variable cell cycle length. *Math. Biosci.* **177&178**, 103-125.

6. A. Bertuzzi, A. Fasano and A. Gandolfi, A free boundary problem with unilateral constraints describing the evolution of a tumour cord under the influence of cell killing agents, submitted.

7. M.I.G. Bloor and M.J. Wilson (1997) A mathematical model of a micrometastasis. *J. Theor. Med.* **1**, 153-168.

8. M.I.G. Bloor and M.J. Wilson (1999) The non-uniform spatial development of a micrometastasis. *J. Theor. Med.* **2**, 55-71.

9. M.J. Boyer and I.F. Tannock (1998). Cellular and molecular basis of chemotherapy. In *The Basic Science of Oncology*, I.F. Tannock and R.P. Hill (Eds), New York: McGrow-Hill, pp. 350-369.

10. C.J.W. Breward, H.M. Byrne and C.E. Lewis (2001) Modelling the interactions between tumour cells and a blood vessel in a microenvironment within a vascular tumour. *Eur. J. Appl. Math.* **12**, 529-556.

11. C.J.W. Breward, H.M. Byrne and C.E. Lewis (2002) The role of cell-cell interactions in a two-phase model for avascular tumour growth. *J. Math. Biol.* **45**, 125-152.

12. R.G. Bristow and R.P. Hill (1998) Molecular and cellular basis of radiotherapy. In *The Basic Science of Oncology* (eds. I.F. Tannock and R.P. Hill), New York: McGraw-Hill, pp. 295-321.

13. J.M. Brown and B.G. Siim (1996) Hypoxia-specific cytotoxins in cancer therapy. *Semin. Radiat. Oncol.* **6**, 22-36.

14. H.M. Byrne and M.A.J. Chaplain (1995) Growth of nonnecrotic tumors in the presence and absence of inhibitors. *Math. Biosci.* **130**, 151-181.

15. H.M. Byrne and M.A.J. Chaplain (1996) Growth of necrotic tumors in the presence and absence of inhibitors. *Math. Biosci.* **135**, 187-216.

16. J.J. Casciari, S.V. Sotirchos and R.M. Sutherland (1992) Variations in tumor cell growth rates and metabolism with oxygen concentration, glucose concentration, and extracellular pH. *J. Cell. Physiol.* **151**, 386-394.

17. J.D. Chapman, D.L. Dugle, A.P. Reuvers, B.E. Meeker and J. Borsa (1974) Studies on the radiosensitizing effect of oxygen in Chinese hamster cells. *Int. J. Radiat. Biol.* **26**, 383-389.

18. S. Cui and A. Friedman (2001) Analysis of a mathematical model of the growth of necrotic tumors. *J. Math. Anal. Appl.* **255**, 636-677.

19. Z. Darzynkiewicz, G. Juan, X. Li, W. Gorczyca, T. Murakami and F. Traganos (1997). Cytometry in cell necrobiology: analysis of apoptosis and accidental cell death (necrosis). *Cytometry* **27**, 1-20.

20. J. Dyson, R. Villella-Bressan and G. Webb, The steady state of a maturity structured tumor cord cell population, in press.

21. K.H. Falkvoll (1990) The relationship between changes in tumour volume, tumour cell density and parenchimal cord radius in a human melanoma xenograft exposed to single dose irradiation. *Acta Oncol.* **29**, 935-939.

22. J. Folkman (1995) Angiogenesis in cancer, vascular, rheumatoid and other disease. *Nature Med.* **1**, 27-31.

23. H.B. Forrester, C.A. Vidair, N. Albright, C.C. Ling and W.C. Dewey (1999) Using computerized video time lapse for quantifying cell death of X-irradiated rat embryo cells transfected with c-*myc* or c-Ha-*ras*. *Cancer Res.* **59**, 931-939.

24. H.P. Greenspan (1972) Models for the growth of a solid tumor by diffusion. *Stud. Appl. Math.* **51**, 317-340.

25. D.G. Hirst and J. Denekamp (1979) Tumour cell proliferation in relation to the vasculature. *Cell Tissue Kinet.* **12**, 31-42.

26. D.G. Hirst, J. Denekamp and B. Hobson (1982) Proliferation kinetics of endothelial and tumour cells in three mouse mammary carcinomas. *Cell Tissue Kinet.* **15**, 251-261.

27. D.G. Hirst, V.K. Hirst, B. Joiner, V. Praise and K.M. Shaffi (1991) Changes in tumour morphology with alterations in oxygen availability: further evidence for oxygen as a limiting substrate. *Br. J. Cancer* **64**, 54-58.

28. J. Holash, P.C. Maisonpierre, D. Compton, P. Boland, C.R. Alexander, D. Zagzag, G.D. Yankopoulos and S.J. Wiegand (1999) Vessel cooption, regression, and growth in tumors mediated by angiopoietins and VEGF. *Science* **284**, 1994-1998.

29. L. Holmgren, M.S. O'Reilly and J. Folkman (1995) Dormancy of micrometastases: balanced proliferation and apoptosis in presence of angiogenesis suppression. *Nature Med.* **1**, 149-153.

30. T.L. Jackson (2002) Vascular tumor growth and treatment: consequences of polyclonality, competition and dynamic vascular support. *J. Math. Biol.* **44**, 201-226.

31. T.L. Jackson and H.M. Byrne (2000) A mathematical model to study the effects of drug resistance and vasculature on the response of solid tumors to chemotherapy. *Math. Biosci.* **164**, 17-38.

32. R.K. Jain (1999) Transport of molecules, particles and cells in solid tumors. *Annu. Rev. Biomed. Eng.* **1**, 241-263.

33. J.M. Joulia, F. Pinguet, M. Ychou, J. Duffour, D. Topart, P.Y. Grosse, C. Astre and F. Bressolle (1997) Pharmacokinetics of 5-fluorouracil (5-FUra) in patients with metastatic colorectal cancer receiving 5-FUra bolus plus continuous infusion with high dose folinic acid (LV5FU2). *Anticancer Res.* **17**, 2727-2730.

34. A.H. Kyle and A.I. Minchinton (1999) Measurement of delivery and metabolism of tirapazamine to tumour tissue using the multilayered cell culture model. *Cancer Chemother. Pharmacol.* **43**, 213-220.

35. S.R. Lubkin, and T. Jackson (2002) Multiphase mechanics of capsule formation in tumors. *J. Biomech. Eng.* **124**, 237-243.

36. G. Majno and I. Joris (1995) Apoptosis, oncosis and necrosis. An overview of cell death. *Am. J. Pathol.* **146**, 3-15.

37. D.L.S. McElwain and P.J. Ponzo (1977) A model for the growth of a solid tumor with non-uniform oxygen consumption. *Math. Biosci.* **35**, 267-279.

38. F. Montalenti, G. Sena, P. Cappella and P. Ubezio (1998) Simulating cancer cell kinetics after drug treatment: application to Cisplatin on ovarian carcinoma. *Phys. Rev. E* **57**, 5877-5887.

39. J.V. Moore, P.S. Hasleton and C.H. Buckley (1985) Tumour cords in 52 human bronchial and cervical squamous cell carcinomas: Inferences for their cellular kinetics and radiobiology. *Br. J. Cancer* **51**, 407-413.

40. J.V. Moore, H.A. Hopkins and W.B. Looney (1980) Dynamic histology of a rat hepatoma and the response to 5-fluorouracil. *Cell Tissue Kinet.* **13**, 53-63.

41. J.V. Moore, H.A. Hopkins and W.B. Looney (1983) Response of cell populations in tumor cords to a single dose of cyclophosphamide or radiation. *Eur. J. Cancer Clin. Oncol.* **19**, 73-79.

42. J.V. Moore, H.A. Hopkins and W.B. Looney (1984) Tumour-cord parameters in two rat hepatomas that differ in their radiobiological oxygenation status. *Radiat. Environ. Biophys.* **23**, 213-222.

43. G. Sena, C. Onado, P. Cappella, F. Montalenti and P. Ubezio (1999) Measuring the complexity of cell cycle arrest and killing of drugs: kinetics of phase-specific effects induced by taxol. *Cytometry* **37**, 113-124.

44. G.D. Smith (1965) *Numerical Solution of Partial Differential Equations*, London: Oxford University Press.

45. I.F. Tannock (1968) The relation between cell proliferation and the vascular system in a transplanted mouse mammary tumour. *Br. J. Cancer* **22**, 258-273.

46. I.F. Tannock (2001) Tumor physiology and drug resistance. *Cancer Metastasis Rev.* **20**, 123-132.

47. I. Tannock, and A. Howes (1973) The response of viable tumor cords to a single dose of radiation. *Radiat. Res.* **55**, 477-486.

48. J.P. Ward and J.R. King (1997) Mathematical modelling of avascular-tumour growth. *IMA J. Math. Appl. Med. Biol.* **14**, 39-69.

49. J.P. Ward and J.R. King (1999) Mathematical modelling of avascular-tumour growth II: Modelling growth saturation. *IMA J. Math. Appl. Med. Biol.* **16**, 171-211.

50. J.P. Ward and J.R. King (2003). Mathematical modelling of drug transport in tumour multicell spheroids and monolayer cultures. *Math. Biosci.* **181**, 177-207.

51. G.F. Webb (2002) The steady state of a tumor cord cell population. *J. Evolut. Equat.*, in press.